PD1-therapy-resistant Terminally Exhausted CD8$^+$T cells promote generation and maintenance of functionally aggressive Cancer Stem Cells

Mohona Chakravarti[1], Sukanya Dhar[1], Saurav Bera[1], Abhipsa Sinha[2], Kamalika Roy[3], Anirban Sarkar[1], Shayani Dasgupta[1], Avishek Bhuniya[1], Akata Saha[1], Juhina Das[1], Saptak Banerjee[1], Manisha Vernekar[4], Chiranjib Pal[3], Neyaz Alam[5], Dipak Datta[2], Rathindranath Baral[1], Anamika Bose[1, 6]*

[1]Department of Immunoregulation and Immunodiagnostics, Chittaranjan National Cancer Institute, 37, S. P. Mukherjee Road, Kolkata-700026, India
[2]Cancer Biology Division, CSIR-Central Drug Research Institute, Lucknow-226031, India
[3]West Bengal State University, Barasat, Kolkata-700032, India
[4]Department of gynecological Oncology, Chittaranjan National Cancer Institute, 37, S. P. Mukherjee Road, Kolkata-700026, India
[5]Department of Surgical Oncology, Chittaranjan National Cancer Institute, 37, S. P. Mukherjee Road, Kolkata-700026, India
[6] Department of Pharmaceutical Technology (Biotechnology)
National Institute of Pharmaceutical Education & Research (NIPER)

*Corresponding Author

Anamika Bose, Ph.D
Assistant Professor
Department of Pharmaceutical Technology (Biotechnology)
National Institute of Pharmaceutical Education & Research (NIPER)
S.A.S. Nagar, Mohali
Punjab-160062; India
E mail: anamikabose2@gmail.com; boseanamika@niper.ac.in
ORCID ID: https://orcid.org/0000-0003-2241-2033
Phone No: +918240393234; +918902268070

Anamika Bose
30/8/2023

PD1-therapy-resistant Terminally Exhausted $CD8^+$T cells promote generation and maintenance of functionally aggressive Cancer Stem Cells

Mohona Chakravarti[1], Sukanya Dhar[1], Saurav Bera[1], Abhipsa Sinha[2], Kamalika Roy[3], Anirban Sarkar[1], Shayani Dasgupta[1], Avishek Bhuniya[1], Akata Saha[1], Juhina Das[1], Saptak Banerjee[1], Manisha Vernekar[4], Chiranjib Pal[3], Neyaz Alam[5], Dipak Datta[2], Rathindranath Baral[1], Anamika Bose[1, 6]*

[1]Department of Immunoregulation and Immunodiagnostics, Chittaranjan National Cancer Institute, 37, S. P. Mukherjee Road, Kolkata-700026, India
[2]Cancer Biology Division, CSIR-Central Drug Research Institute, Lucknow-226031, India
[3]West Bengal State University, Barasat, Kolkata-700032, India
[4]Department of gynecological Oncology, Chittaranjan National Cancer Institute, 37, S. P. Mukherjee Road, Kolkata-700026, India
[5]Department of Surgical Oncology, Chittaranjan National Cancer Institute, 37, S. P. Mukherjee Road, Kolkata-700026, India
[6] Department of Pharmaceutical Technology (Biotechnology)
National Institute of Pharmaceutical Education & Research (NIPER)

*Corresponding Author

Anamika Bose, Ph.D
Assistant Professor
Department of Pharmaceutical Technology (Biotechnology)
National Institute of Pharmaceutical Education & Research (NIPER)
S.A.S. Nagar, Mohali
Punjab-160062; India
E mail: anamikabose2@gmail.com; boseanamika@niper.ac.in
ORCID ID: https://orcid.org/0000-0003-2241-2033
Phone No: +918240393234; +918902268070

Abstract

Heterogeneity within the tumor-infiltrating lymphocytes population limits immunotherapeutic efficacy against cancer. Between two subpopulations of exhausted CD8þ TILs (progeni tor-exhausted; TPEX, terminally exhausted; TTEX), TTEX cells remain unresponsive to anti–programmed cell death protein 1(PD-1) therapy. Deciphering whether and how PD-1 resistant TTEX cells engage in tumor promotion could improve the response to immu notherapy. Here, we report that TTEX cells actively participate in tumor progression by modulating cancer stem cells (CSC). TTEX cells strongly correlated with elevated CSC frequency in poorly immune-infiltrated (CD8þ TIL low) advanced human breast and ovarian carcinomas. TTEX directly upregulated CSC frequency *in vitro*, which was not affected by anti–PD-1 treatment. The TTEX-influenced CSCs were highly clonogenic and exhibited a multidrug resistant phenotype, overexpressing drug efflux pumps like ABCC1 and ABCB1. These CSCs were highly invasive, dis playing increased invadopodia development and elevated cofilin, CXCR4, and matrix metalloproteinase 7 (MMP7) expression. The invasive properties along with epithelial–mesenchymal plasticity of TTEX-educated CSCs increased metastasis in vivo. TTEX increased cell surface levels and activation of VEGFR2 in CSCs, and silencing or inhibition of VEGFR2 reversed the CSC-stimulatory effects of TTEX. LAMP3 and NRP1 on the surface of TTEX stimulated VEGFR2 in CSCs to promote aggressiveness. Cumulatively, these findings suggest that screening patients with carcinoma for both CD8-TILs and TTEX frequency prior to anti–PD 1 therapy could improve patient outcomes. In addition, targeting the LAMP3/ NRP1–VEGFR2 axis could be a therapeutic strategy in advanced patients with carcinoma with limited CD8þ T cell infiltration and high TTEX frequency.

Introduction:

Intra-tumor complexity poses major challenge in successful cancer management. A self-renewing rare subset of stem cells; designated as Cancer Stem Cells (CSCs), fuels such heterogeneity[1]. CSCs remain arrested in a quiescent state; only transiently proliferate to generate heterogeneous malignant tumor bulk, which is generally non-CSC and can seldom foster tumors in xenograft assays[2]. However, this hierarchy is not always maintained; plasticity and de-differentiation of terminally differentiated malignant cells to CSC-like-state is also evident under specific conditions[3-5]. Intra-tumor CSC supportive-niche provides protection from diverse genotoxic hits, by overexpressing ABC-drug efflux proteins, enhancing DNA repair mechanisms, resisting DNA damage, and up-regulating anti-apoptotic proteins[6-7]. Tumor intrinsic hypoxia feeds this flame via up-regulating HIF1α, conferring enhanced therapy resistance; eventually resulting into relapse[8]. CSCs also initiate metastasis and secondary tumor formation by inducing extra-cellular-matrix (ECM) re-organization, epithelial-mesenchymal-transition (EMT), neovascularization, vascular mimicry and seeding at secondary site[9-11].

Substantial evidence suggested the importance of immune cells regulating CSC fate, like, TAM[12], MDSCs[13]and Tregs[14]support CSCs, while NK[15]and γδT[16] cells function against it. Immune-suppressive network increases CSC frequency; stemness and aggressive phenotype [17]. CSC survival gets furthermore ensured due to truncation of effector response from infiltrated $CD8^+$T cells. Within tumor microenvironment (TME), due to prolonged antigenic exposure and presence of immune-suppressive milieu, $CD8^+$T cells undergo hierarchical loss of proliferation and effector functions including secretion of IL-2, TNFα, IFNγ and β-chemokines. At this "exhausted" state, they show a sustained over expression of co-inhibitory receptors, like, PD-1, TIM-3, LAG-3, CTLA-4, and TIGIT. These hypo-responsive-exhausted $CD8^+$T cells fail to regulate tumor growth[18].

Therefore, over the past decade, numerous studies took place to revitalize exhausted $CD8^+$T cells. Several immune checkpoint inhibitors (ICI) like- Pembrolizumab and Nivolumab (anti-PD1), Ipilimumab (anti-CTLA-4), Atezolizumab (anti-PDL1) underwent clinical trial and showed positive therapeutic response[19]. However, variance within the targeted cell limited their success rate. Recent reports in human melanoma have shone light on such incongruity; existence of two sub-populations, early-state progenitor exhausted (T_{PEX}) ($CD8^+PD1^+TCF1^+$), and late-state terminally exhausted (T_{TEX}) ($CD8^+PD1^+TCF1^-$) within exhausted $CD8^+$T cell pool. While T_{PEX} cells responded to anti-PD1-therapy, T_{TEX} cells did not[20]. However, whether these subsets exist similarly in other solid tumors remains unknown. Moreover, their behavior within TME, particularly their possible involvement in tumor advancement via CSC-modulation remains unexplored.

Here, in this study, we have found co-existence of both T_{PEX} and T_{TEX} population within infiltrated-$CD8^+$TILs of human breast and ovarian carcinoma and murine melanoma. Notably, a striking positive correlation between T_{TEX} cells and CSCs was observed, indicating their pro-tumor behavior. Furthermore, *in-vitro* and *in-vivo* studies revealed that PD1-therapy-resistant T_{TEX} cells directly generate an aggressive CSC-variant, eventually leading to invasion and hepatic metastasis. This aggression was neutralized by targeting LAMP3/NRP1-VEGFR2 cascade.

Materials and Methods:

Reagents and antibodies: DMEM high-glucose, MEM, RPMI-1640, DMEM: F12K (1:1)media andfetal bovine serum (FBS) were procured from Hi-Media (Mumbai, India). B-27TM Supplement (50X) was procured from Gibco (Waltham, USA). Recombinanthuman epidermal growth factor(rEGF) and recombinant human basic fibroblast growthfactor (rbFGF) were obtained fromMerck-Milipore (Darmstadt, Germany). VEGFR2Kinase Inhibitor I, PD-1/PD-L1 small molecule inhibitor 1 (Abcam, Cambridge, UK);Streptavidin Particles Plus-DM, antibodies for ELISA (BDBiosciences, SanJose, CA)were procured from different vendors as indicated in parentheses. Heparin, Sunitinibmalate, FluoroshieldTM with DAPI and β-mercaptoethanol were purchasedfrom Sigma-Aldrich (Missouri, USA).

Human Solid tumors: Post-operative tumor tissue(breast, n=22; ovary, n=11) andtumor-adjacenttissues with proven histopathological normalcy were obtained fromChittaranjan National CancerInstitute (CNCI), Kolkata, India following approval fromInstitutional Ethical Committee (Ref:CNCI-IEC-RB-2019-6). For breast carcinoma, TNMstaging and for ovarian carcinoma FIGO classification is provided.

Mice and tumors: Wild-type (Wt) female C57BL/6 mice (age: 4-6 weeks; body weight:18-22 g on average) were obtained from Institutional Animal Care and MaintenanceDepartment. Female nude mice of Crl:NU-Foxn1nu strain in Balb/C background (age: 4-6 weeks,body weight: 18-22 g on average) were obtained from CSIR-Central DrugResearch Institute,Lucknow, India. All experimental mice were housed in pathogen freeenvironment; fed withautoclaved dry pellets (Epic Laboratory, West BengalGovernment, Kalyani, India) and water ad libitum. Experimental protocol was approvedby the Institutional Animal Care and EthicsCommittee (Approval No.: IAEC-1774/RB-15/2017/2 and IAEC-1774/RB-19/2017/15).

To establish solid melanoma tumor, B16-F10 cells ($1\times10X^5$)/mice were injectedsubcutaneously in the lower right flank of C57BL/6 mice. Tumor growth was monitoredtwice per week bycaliper measurement and presented as mm^2 (length×width).

Cell lines and culture: B16-F10, MCF7, MDAMB-231, 4T1 cell lines were obtainedfrom National Centre for Cell Sciences (NCCS), Pune, India. Cell line authentication viaSTR profiling was conducted by cell repository and maintained as per instructions. All experiments were conducted within 7-10 passages afterthawing them.

Tumor tissue processing for flow-cytometry, cryo-sectioning: Tumor tissue processing were carried out following methods described elsewhere (19).

Tumor cell lysate preparation: Tumor lysate was yielded from freshly prepared singlecell suspension of solid tumor tissue samples. Cells ($2x10^7$) were suspended in 1 mlPBS andsubjected to 7-10 cycles of freeze (in liquid nitrogen) and thawing (37°C waterbath).

Generated lysate wasextracted by centrifugation and filter sterilization. Proteincontent was determined by Bradford assay.

Preparation of tumor supernatant: Tumor supernatants were developed from mediaofconfluent cultures of MCF7/MDAMB-231/4T1 cells. Media from these adherentmonolayerswere collected, centrifuged and filter-sterilized prior to use.Cryo-sectioning: Previouslyprepared fixed tissue samples were embedded in optimalcutting temperature compound (OCTcompound). The embedded frozen tissue samples weresectioned (5μM) on a Cryostat, collected on poly-l-lysinecoated slides and storedat -80oC until further use.

Histology and HE staining: Histopathology was carried out following methods described elsewhere (19)

Purification of CSCs and $CD8^+$T cells by magnetic cell sorting: Target cellsuspensions weremagnetically labeled with CD8/CD44/CD24/Lineage-cocktailantibodies as per requirement. Cellpurification was followed according to themanufactures protocol (Microbead kit, MiltenyBiotech, Germany). Cell purity waschecked by flow-cytometry.Co-culture and Transwell assay: Purified CD8+T cell subtypes were cultured in1:1MEM and RPMI complete media with MCF7/MDAMB231/4T1 cells at 5:1ratio inpresence/absence of 0.4 μMtranswell membrane for 48 hrs.After incubation period, T cell suspension was removed and adherentMCF7/MDAMB231/4T1 population was trypsinized, centrifuged and collected fordownstream assays.

RT-PCR and Quantitative PCR:RT-PCR and quantitative PCR were done following methos described elsewhere (19)

Immunofluorescence microscopy and analysis: Immunofluorescence microscopy was carried out using protocol described earlier (19). Fluorescence intensity wasevaluated by Image-J software. The corrected total cellfluorescence (CTCF) has been computed from:CTCF = Integrated density−(Area of selected cell × Mean fluorescence of backgroundreadings).

Flow-cytometry: Flow-cytometry was carried out using protocol described earlier (19)

ELISA: Antigens harvested from experimental groups were immobilized on 96-wellmicrotiterplate; assay was conducted as previously described(19)

Matrigel invasion assay: Post co-culture, magnetically purified CSCs suspended inbasalmedium was layered on top of the matrigel coated transwell inserts (8μm). Aseptically the cell suspension containing insertswere loaded ontochemo-attractant containing 24-wells and incubated for 22-hours. Invaded cells adhered tothe membrane was fixed in paraformaldehyde, permeablized by absolute methanol and stainedwith 0.2% crystal violet. Migrated cellswere imaged and quantified from five random fields. Invasion index was calculated from:Percentage of invasion = % of invasion of control cells / %of invasion of test cells.

Tumorsphere assay:IMag purified CSCs($1x10^4$) from in-vitro culture were seeded in ultra-lowadherent plates in 2 ml CSC enrichment media and incubated for 7 days. Number of

tumorspheres from five random spots per well was counted and micrographed. Area of tumorspheres was documented and tabulated using ImageJsoftware.

Colony formation assay on soft agar: Cells (5 x 10^3) were grown on upper layer ofsoft agar (0.35% agarose) blended with cell culture medium. This layer was rested on abottom layerconsisting of 0.7% agar and cell culture medium. The culture setup wasincubated for 21 dayswith media supplementation at every 4 days. Finally, totalnumbers of colonies were quantifiedfrom five randomly taken micrographs/ well(original magnification, × 10). For envision,colonies were fixed in 2%paraformaldehyde, stained with 0.04% crystal violet and 2% ethanolin PBS.

VEGFR2 neutralization: Cancer cells were primarily seeded to reach 70% confluency; then transferred to 2% FBS containing culture media for overnight. On following day, cells weretreated separately with 1nM Sunitinib and 1nM VEGFR2 inhibitor for 24hours.

Cell Cycle Analysis: Cells were harvested, fixed in chilled 70% ethanol while vortexing, followed by incubation at −20◦C overnight. Cells were washed twice with PBS containing 0.1%sodium azide, followed by 50µL(100 ng/mL)RNase treatment. Cellswere stained with 200µL(50µg/mL)PI to analyze flow-cytometrically immediately.

Western Blot: To monitor different signaling molecules cellular lysate (30-50 µg) was separated on 12% SDS-PAGE western blotting was carried out as described (21)

SiRNA mediated silencing: siRNA for human-LAMP3 and human-NRP1 wereconstructed *invitro* using Silencer R siRNA construction kit (Life Technologies,USA)according to themanufacturer's protocol.Both the target specific siRNA and scramble control siRNA were addedto in-vitro setup to a final concentration of 50nM to the 2 hr-serum starved cells inpresence of lipofectamine-2000 reagent.

Statistical analyses: All results represent the mean±SD of data obtained from eitherone (n=6 for*in-vivo*) or three to six (for *in-vitro*) independent experiments. Statisticalsignificance was established from unpaired Student t-test (for two groups) or one-way/two-way analysis of variance. Positive and/or negative correlation was deducedfrom Pearson Correlation coefficient. All statistical analysis and heatmaps were generated by GraphpadPrism 8.4.2 software(Graphpad Software, San Diego, CA,USA).Experimental groups attaining $p \leq 0.05$ consideredas significant.

Results:

Exhausted $CD8^+$T cell positively correlates to CSC frequency in human advancedcarcinomas:

To investigate the influence of overall exhausted $CD8^+$T cell population on CSCs of solid TME,pre-treatment tumor-biopsies of breast (n=34) and ovarian (n=11) origin were screened for exhausted $CD8^+$T ($Lin^+CD8^+PD1^+$) cells and CSCs ($Lin^-CD44^+CD24^-$ in breast and $LinCD44^+CD133^+CD117^+$ in ovary). Lineage-sorting followed by flow- cytometric

analysisidentified both populations in all biopsies. It was found that aggressive breast and ovariancarcinoma subsets (invasive-ductal-CaBr and advanced- stage-III-OvaCa) contained a higherfrequency of exhausted $CD8^{+}PD1^{+}$T cells and CSC populations in comparison to tumoradjacent-histopathologicallynormal tissues. These frequencies are much lower in less-aggressivecarcinoma subset (in situ-CaBr in breast and early-stage-I/II-OvaCa in ovary). Furthermore, a strong positive correlation between exhausted $CD8^{+}PD1^{+}$ cells and CSCs was noted across all breast (r = 0.8955) and ovarian (r = 0.9284) carcinoma biopsies.

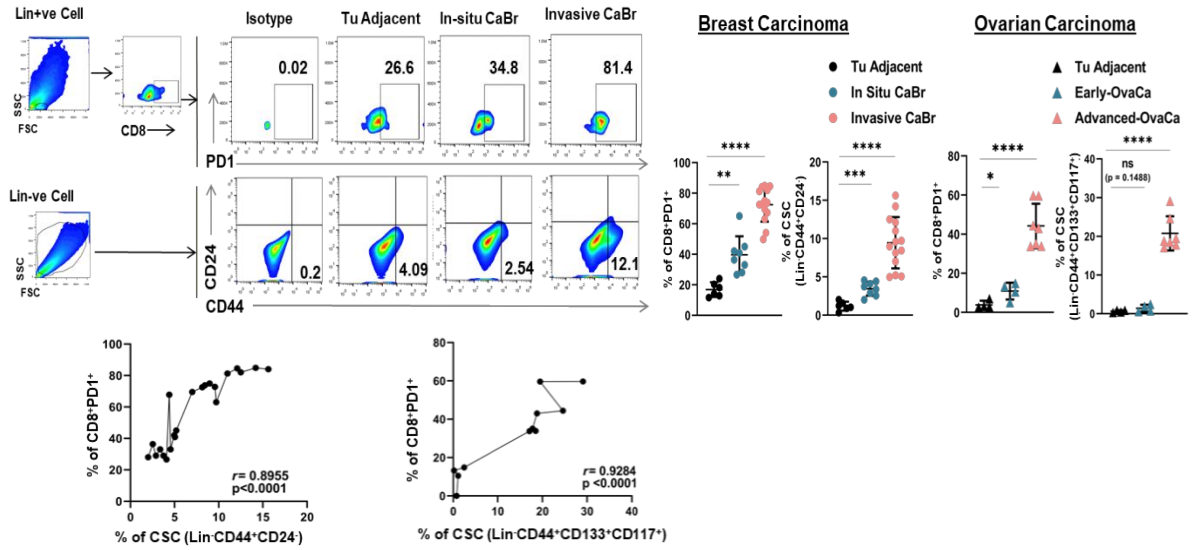

Figure 1: CSC frequency positively correlates with exhausted CD8T cell population within human-carcinoma TME. Representative pseudocolor-flow-plots for $Lin^{+}CD8^{+}PD1^{+}$ and $Lin^{-}CD44^{+}CD24^{-}$ population in CaBr biopsy samples. Scatterplots represent individual percentage of respective populations with mean± SD in all groups (n= 34 for breast, n=11 for ovary); unpaired parametric t-test. Positive co-relation between exhausted $CD8^{+}$T-cells ($Lin^{+}CD8^{+}PD1^{+}$) and CSC ($Lin^{-}CD44^{+}CD24^{-}$ /$Lin^{-}CD133^{+}CD44^{+}CD117^{+}$) illustrated by scatter plots, where r represents Pearson correlation coefficient, followed by two-tailed p value.*p<0.05, **p < 0.01, ***p < 0.001, ****p < 0.0001, ns: not significant are indicated.

Terminally exhausted $CD8^{+}$T cell positively correlates to CSC frequency in human advanced carcinomas with poor immune-infiltration:

Now, to assess the existence of possible sub-populations within exhausted $CD8^{+}$T-TIL pool and their probable role in influencing CSCs, studies were undertaken on advanced stage breast (n=22) and ovarian carcinomas (n=9). They were primarily categorized into hot ($CD8^{+}$T-TIL >6%) and cold ($CD8^{+}$T-TIL <6%) tumors and screened for progenitor exhausted (T_{PEX}) *($Lin^{+}CD8^{+}PD^{+}TCF1^{+}$)* and terminally exhausted (T_{TEX}) (*$Lin^{+}CD8^{+}PD1^{+}TCF1^{-}$*) population along with CSCs. Flow-cytometric analysis after lineage-sorting revealed that two sub-sets T_{PEX} and T_{TEX} do exist within tumor-infiltrated $CD8^{+}$T cell population. It was observed that in cold tumors, both T_{TEX} and CSC frequency was elevated in comparison to hot tumors. Moreover, T_{TEX} cells followed a negative correlation with infiltrated-$CD8^{+}$T cell frequency (r =-0.7906 in breast and r =-0.9269 in ovarian carcinoma). While relative frequency of T_{TEX} over T_{PEX} cells

positively correlated with CSC frequency (r = 0.9214 in breast, r = 0.8809 in ovary), indicating a possible CSC-uprising role of T_{TEX} in cold-tumors.

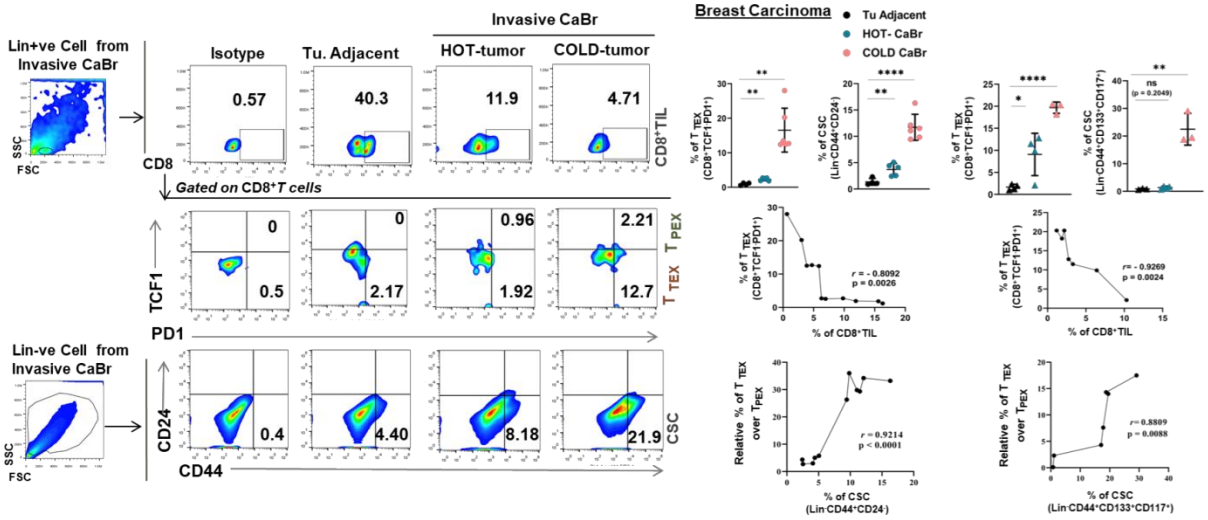

Figure 2: CSC population positively correlates with T_{TEX} frequency in human-carcinoma cold-TME: Pseudocolor-flow-plots for tumor-infiltrated $CD8^+$T cells, Progenitor Exhausted (T_{PEX}) $Lin^+CD8^+PD1^+TCF1^+$, Terminally Exhausted (T_{TEX}) $Lin^+CD8^+PD1^+TCF1^-$ cells and CSCs for tumor-adjacent-normal, hot and cold tumors in advanced carcinomas. Scatterplots represent individual percentage of respective populations with mean ± SD in all groups (n= 22 for breast, n=9 for ovary); unpaired parametric t-test. Negative correlation between CD8TIL with T_{TEX} and positive correlation between relative percentages of T_{TEX} with % of CSC represented by scatter plots. r represents Pearson correlation coefficient, followed by two-tailed p value.*p<0.05, **p < 0.01, ***p < 0.001, ****p < 0.0001, ns: not significant are indicated.

Immunophenotyping/ Characterization in-vitro generated exhausted CD8$^+$T cell sub types:

Initially, exhausted CD8T cell subsets- T_{PEX} and T_{TEX} cell population was generated from PBMC of healthy donors and murine spleenocytes *in-vitro*. Briefly, the lymphocytes were chronically stimulated with breast cancer specific antigens while simultaneously being pulsed with antigen-loaded DCs to induce the exhaustion. To define the phenotype and outline the exhaustion status of these two subsets, RT-PCR and flow-cytometry was performed. Both T_{PEX} and T_{TEX} were found to be enriched for exhaustion signature. Moreover, these cells showed separate and distinct gene expression profiles; $CD8^+T_{PEX}$ displaying $PD1^+TIM3^-TCF1^+CXCR5^{low}IFN\gamma^{low}TOX^{low}KLRG1^-Eomes^-$ phenotype while T_{TEX} cells retained $PD1^+TIM3^+TCF1^-CXCR5^-IFN\gamma^{low}TOX^{high}KLRG1^-Eomes^+$ phenotype. Flowcytometric analysis also supported their time dependent generation and changes in phenotype. For functional assay, after culturing with cancer-cell-lines, both T_{TEX} and T_{PEX} exhibited lower expression of *perforin*, *granzyme-B* in comparison to activated $CD8^+$ T cells, attributing to their exhausted state.

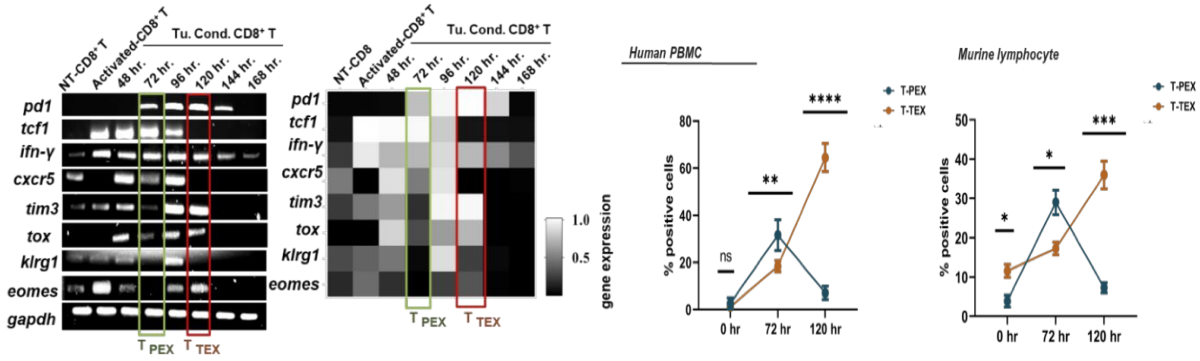

Figure 3: In-vitro generation of exhausted CD8T cell subtypes – T_{TEX} and T_{PEX}. Genetic-profiling of T_{PEX} and T_{TEX}pool via RT-PCR, quantified gene expression intensities are represented by heat-maps, with dark color denoting weak expression and light color denoting strong expression respectively. Scatter plots representing mean±SD for T_{PEX} and T_{TEX} frequency across time points. Statistical significance drawn by two-way ANOVA followed by Tukey's multiple comparison test (n=6).*p<0.05, **p<0.01, ***p<0.001, ****p<0.0001, ns: not significant are indicated.

Terminally exhausted CD8$^+$ T cells induce generation of CSCs:

Principally, *in vitro* generated T_{PEX} and T_{TEX} cells were co-cultured with MCF7 (*human luminal A CaBr cell line*), MDAMB-231 (*human TNBC CaBr cell line*) cells and 4T1 (*murine-TNBC CaBr cell line*) for 48 hours to study their direct impact. Post co-culture, CSC frequency was evaluated via flowcytometry. A significant surge in CSC percentage was noted in presence of T_{TEX} with respect to no-treatment-control. This CSC-elevation wasobserved in all three cancer-cell-lines propagated on both monolayer and 3D-CSC-enrichment setting. However, the aforesaid CSC elevation was marginallylower when cultured with T_{PEX}.

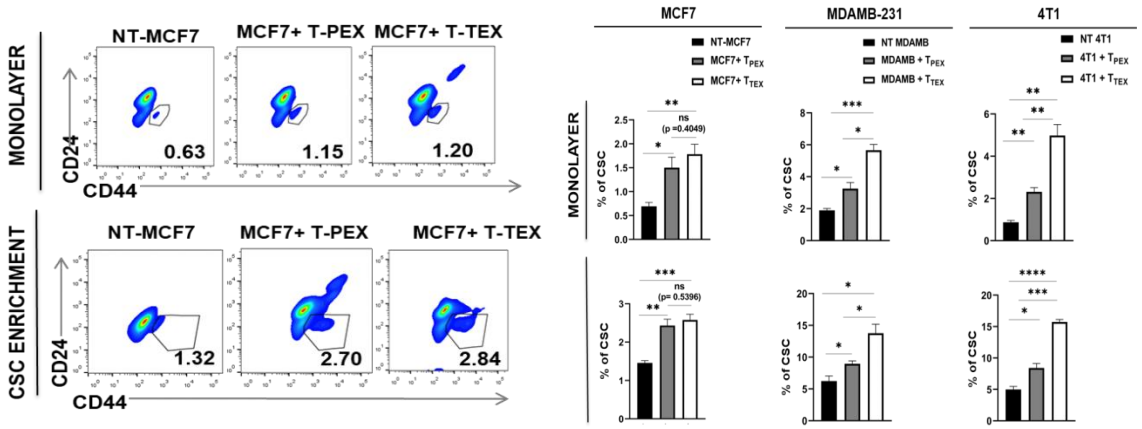

Figure 4: T_{TEX} cells actively upregulate CSC frequency: Pseudocolour flow-cytometric plots representing changes in CSC-frequency in MCF7 due to T_{PEX} and T_{TEX} population. Summary-bar-diagrams represents CSC frequency in NT-control, Cancer cell with T_{PEX} and Cancer cell with T_{TEX} group across MCF7, MDAMB-231 and 4T1 cell-lines keeping mean±SD. Statistical significance was calculated by unpaired-T-test (n=6).*p<0.05, **p < 0.01, ***p < 0.001, ****p < 0.0001, ns: not significant are indicated.

T_{TEX} mediated CSC upregulation is non-remediable to anti-PD1 therapy:

To ascertain the weather anti-PD1 therapy could be used to counteract the T_{TEX} mediated CSC-upregulation, co-culture was conducted in presence and absence of PD1-PDL1 interaction inhibitor (ICI agent) and CSC frequency was analyzed. Our study revealed differential response of T_{TEX} and T_{PEX} to anti-PD1 therapy. While ICI administration significantly brought down percentage of CSC (2.04 % to 1.36 %) in T_{PEX} cohort, CSC population was maintained in a static elevated state (2.17 % to 2.12%) in T_{TEX} group. Thus, it can be said that both T_{PEX} and T_{TEX} contribute directly to CSC elevation, however, only T_{PEX} activity can be counteracted by ICI therapy.

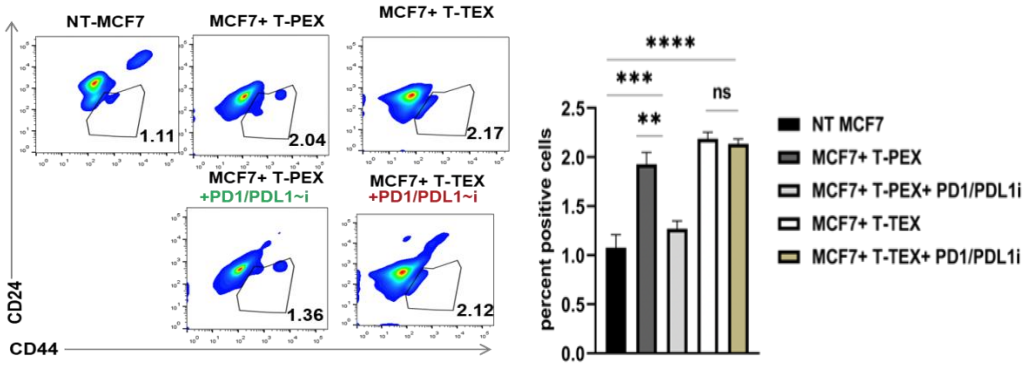

Figure 5: PD1 therapy fails to bring down T_{TEX} induced CSC upregulation: Flowcytometric plots displaying differential response of T-$_{PEX}$ and T-$_{TEX}$ to PD1 blockade, in terms of CSC upregulation in MCF7 cell-line. Bar diagrams depict mean± SD for CSC frequency across all groups. Statistical significance was drawn on the basis of one-way ANOVA followed by Tukey's multiple comparison test (n=6). *p<0.05, **p < 0.01, ***p < 0.001, ****p < 0.0001, ns: not significant are indicated.

T_{TEX} influenced CSCs are aggressive, resistant; remain in a hybrid EMT-MET state:

RT-PCR analysis of MDR-phenotype regulating genes like *bcrp1*, *abcc1*, and *abcb1* revealed an upsurge in *abcc1* and*abcb1* in CSCs under the influence of T_{TEX}. Analyses of gene expression profile of EMT-state have revealed that T_{TEX} influenced CSCs remain in transitory phase between epithelial and mesenchymal lineages. They simultaneously display mesenchymal state with elevated *twist1*, *twist2* expression and low expression of *e-cadherin*; along with low expression of *vimentin, slug and snail*, projecting epithelial state. In chemokine receptor profile analysis, elevation in CXCR4 and MMP7 amidst CCR7, CXCR3, CXCR5, MMP2, MMP9 and MMP11 was found. Further study of sub-cellular distribution of CXCR4 by immunofluorescence microscopy revealed a strong nuclear localization of CXCR4 within T_{TEX} influenced CSCs. Cellular CXCR4 intensity was also strongly elevated in CSCs influenced by T_{TEX}.

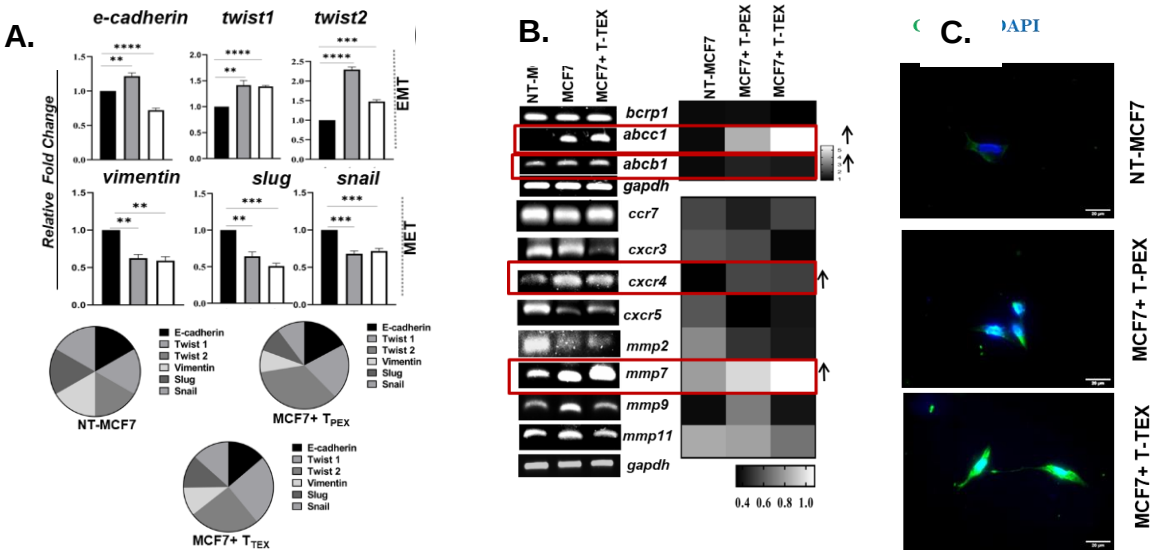

Figure 6: Characterization of T_{TEX} influenced CSCs:A.EMT-MET phenotype analysis of altered CSCs by qRT-PCR. Relative fold changes are represented by summary-bars (mean± SD), with statistical significance drawn from unpaired t-test (n=6). Cumulative EMT-MET-profile of CSCs from respective groups is represented by parts-of-whole-pie-chart. B. mRNA expression of MDR-phenotype regulating genes and chemokines by RT-PCR. Quantified values are represented by heatmaps (mean± SD). C. Representative immune-fluorescence micrographs at 100x magnification for CSCs stained with CXCR4-FITC are provided CSCs.*p<0.05, **p < 0.01, ***p < 0.001, ****p < 0.0001, ns: not significant are indicated.

T_{TEX} influenced CSCs are highly invasive:

T_{TEX} influenced CSCs uptake a very linear invasive morphology with increment incellular length and reduction in cellular width. To assess their invasive potential,matrigel-invasion assay was performed, which disclosed strong invasive vigor in T_{TEX}influenced CSCs. To ascertain how the cytoskeleton is aiding in this invasion, an actin-binding-cytoskeletal protein Cofilin was

analyzed. Immunofluorescence microscopyrevealed different sub-cellular distribution of Cofilin across all test-groups particularlywith increased nuclear expression within T_{TEX} influenced CSCs. This study alsodisplayed elongation of both cytosol and nucleus and also, supporting development ofinvadopodia in T_{TEX} influenced CSCs.

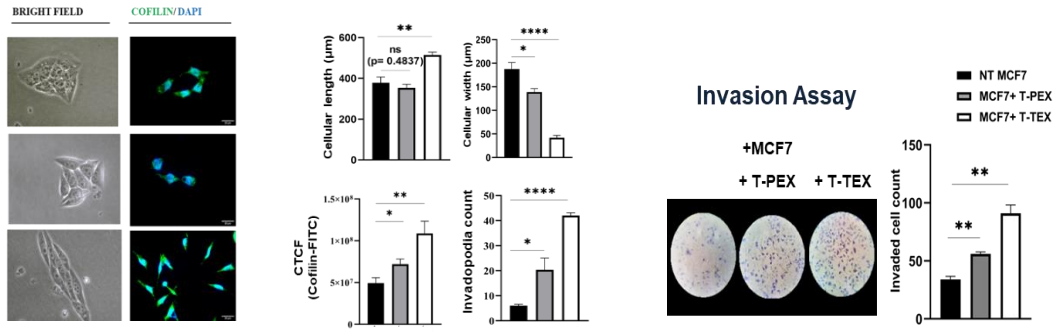

Figure 7: T_{TEX} influenced CSCs are invasive in nature:A. Representative bright-field and immune-fluorescence micrographs at 100x magnification for CSCs stained with Cofilin-FITC are provided. Cellular length, width, Corrected total cell fluorescence intensity (CTCF) and number of invadopodias were quantified and displayed as column graph (mean± SD). B. Representative micrographs for matrigel-invasion assay of isolated CSCs, from each group. Invaded cells quantified and displayed as mean± SD in the column graph, statistical significance drawn from unpaired t-test (n=4).*p<0.05, **p < 0.01, ***p < 0.001, ****p < 0.0001, ns: not significant are indicated.

T_{TEX} influenced CSCs are clonogenic and metastatic:

CSCs were primarily magnetically sorted post co-culture and plated into plated in i*n-vitro* 7-day-tumorsphere assay and 21-day soft agar assay. T_{TEX} influenced CSCs showed increased sphere formation in tumorsphere medium as well as increased colony formation in semi-solid agar plate.

In the *in-vivo* study,1 x10^4 CSCs were isolated and purified from 4T1- T_{PEX} /T_{TEX} *in-vitro* co-culture and inoculated in the mammary fat pad of athymic nude mice for tumor development and observed for possible metastasis. After 25 days of tumor inoculation, liver metastasis was found in mice inoculated with $CD8^+T_{PEX}$influenced CSCs. The liver parenchyma found to be heavily disrupted and necrotic which can be also viewed from HE staining.

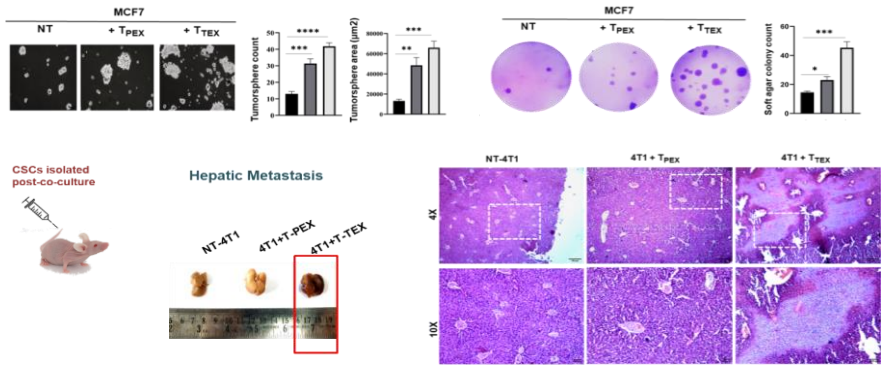

Figure 8: T_{TEX} influenced CSCs show high clonogenecity and hepatic metastasis. A. *In-vitro*, CSCs magnetically sorted post-co-culture and plated for tumorsphere assay. Representative images for all three groups are provided. In bar-graph, mean± SD for tumorsphere count and size is indicated. Statistical significance is inferred from unpaired t-test (n=6). B. *In-vitro*, post-coculture sorted CSCs were plated for soft agar assay. Representative photographs for developed colonies in each group for 3 cell-lines are provided. Number of colonies (mean± SD) is displayed by column-bars. Statistical significance is calculated from unpaired t-test (n=4). C. *In-vivo*, CSCs isolated from 4T1+/- T_{PEX}/T_{TEX} co-culture was subcutaneously injected into mammary-fat-pad of athymic nude mice for development of tumor and observed for possible metastasis. C. Representative photograph of metastatic spread in harvested and formalin-fixed liver tissue across all groups (n=6 mice per group). D. Representative micrographs of Hematoxylyn-Eosin stained liver tissue across all groups. (n=6 mice per group). *p<0.05, **p < 0.01, ***p < 0.001, ****p < 0.0001, ns: not significant are indicated.

T_{TEX} influenced CSC aggression is controlled by stemness regulatory transcription factors:

Since all of the CSCs attributes are primarily regulated by transcription factors like, *oct4*, *sox2*, *klf4*, and *nanog*, their status was evaluated by q-PCR. Significant upsurges in all of these factors were observed in presence of T_{TEX}. *aldh1* regulating stem-cell metabolism was also upregulated in T_{TEX} induced CSCs.

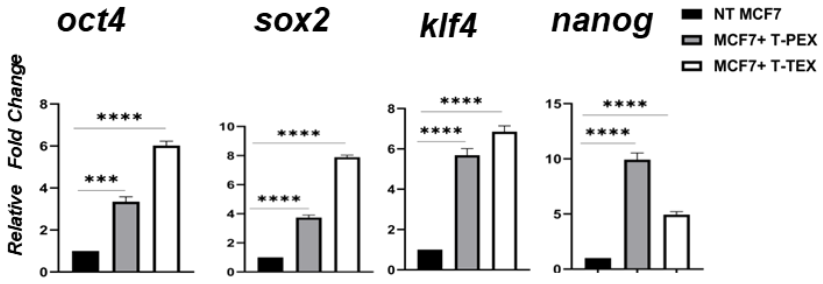

Figure 9: T_{TEX} brings CSC aggression by enhancing stemness regulatory transcription factors. $T_{PEX/TEX}$ influenced CSCs were isolated and evaluated for stemness regulating genes *oct4, sox2, nanog, klf4, aldh1* via qRT-PCR. Relative fold changes are represented by summary-bars (mean± SD). Statistical significance was calculated by unpaired- t-test (n=6).

T_{TEX} induced CSC generation requires cellular contact:

To identify the possible mode of action, co-cultures were performed in two different setups. In one setup, $T_{PEX/TEX}$ and cancer cells were physically separated using a 0.4µm transwell membrane, so that target population can only communicate via cellular-secretions (contact-independent). While, in another; both the cells were cultured in same well, so that the receptor-ligand interaction can take place (contact-dependent). Post co-culture, CSC-percentage was analyzed via flow-cytometry. It was found that T_{TEX} induced CSC hike was only evident in contact dependent setup. To further validate, co-culture supernatants from contact-dependent-setup were analyzed by ELISA for IL-2, IL-4, IL5, IL-6, IL-10, IL-12, IL-13, IFN-γ, TGF-β and TNF-α and it was noted that T_{TEX} mediated CSC upregulation does not invoke activity of any of these cytokines.

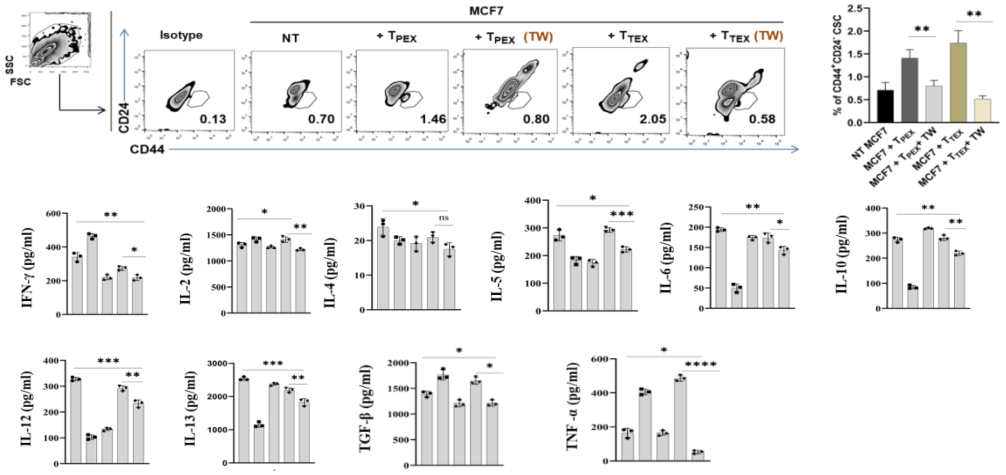

Figure 10: T_{TEX} mediated CSC upregulation is contact dependent. A. Flowcytometric zebra-plots for CSC frequency in co-culture setups with and without transwell membrane keeping no-treatment cancer cell lines as control Summary-bar-graphs are displayed on the right, presenting mean± SD for CSC frequencies in respective groups. Statistical significance is calculated from unpaired t-test (n=4). B. Co-culture supernatants were assessed against no-treatment cancer cells and $CD8^+$ T-PEX/TEX cells. Summary bar represents mean± SD for pg/ml cytokine secretion (n=3). *p<0.05, **p < 0.01, ***p < 0.001, ****p < 0.0001, ns: not significant are indicated.

T_{TEX} instigates VEGFR2 on CSC surface:

Since our previous results direct towards a physical contact dependent CSC upraise for T_{TEX} cells. CSCs were screened for the receptor status of classical receptor-ligand based signaling pathways regulating CSC-fate. Our qRT-PCR analysis for *wnt3a*, *notch1*, *notch4* denied involvement of the any of the said receptors. However, selective involvement of VEGFR2 was found in T_{TEX} influenced CSCs. Their involvement was further validated conducting co-culture in presence of Sunitinib (inhibits both VEGFR1 and VEGFR2) and selective VEGFR2 inhibitor (VEGFR2 Kinase Inhibitor I, ab145888). Flowcytometry revealed that both the inhibitor treatments significantly lowered frequency of CSC; however, VEGFR2-inhibitor was more effective (lowering CSC from 2.72% to 1.24%) than Sunitinib (lowering CSC from 2.72% to 1.81%), indicating a VEGFR2 mediated CSC-upraise.

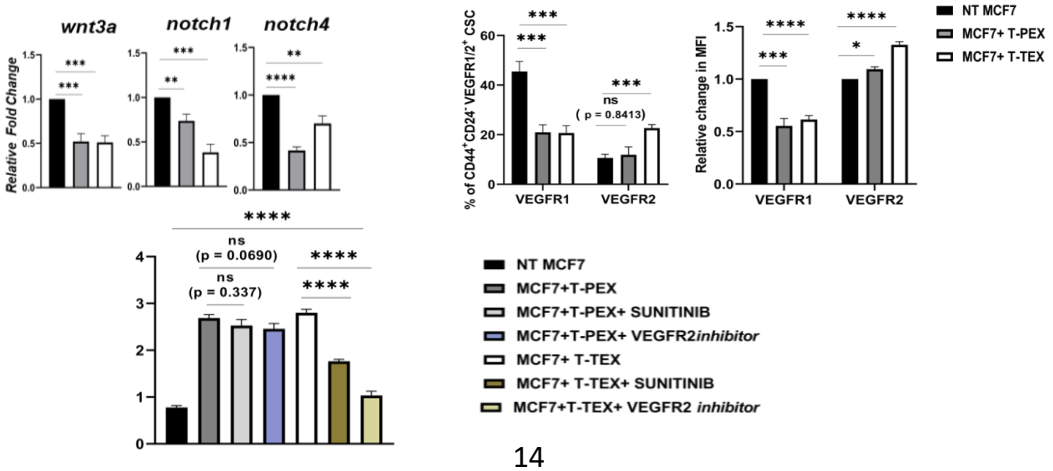

Figure 11: T_{TEX} exerts through VEGFR2 on CSC surface. A. Analyzing the status of CSC-fate-regulating cell-surface receptors within CSC-population via q-RT PCR. Relative fold changes in gene expression across all groups are displayed via bar-graphs (mean± SD); unpaired t-test (n=5). B. Percentage of $CD44^{+}CD24^{-}VEGFR1^{+}/R2^{+}$ population and relative change of MFI of VEGFR1 and VEGFR2 within $CD44^{+}CD24^{-}$ CSC pool is represented by bar-graphs (mean± SD); one-way ANOVA followed by Tukey's multiple comparison test (n=4). C. Summary bars depicting CSC frequency for MCF7 and T-$_{PEX}$/T-$_{TEX}$ co-culture in presence and absence of 1nM Sunitinib and small-molecule-VEGFR2-inhibitor. Column graphs represent mean± SD; one-way ANOVA followed by Tukey's multiple comparison test (n=5). *p<0.05, **p < 0.01, ***p < 0.001, ****p < 0.0001, ns: not significant are indicated.

T_{TEX} influences CSC aggressiveness via LAMP3/NRP1-VEGFR2 axis:

Finally, the trans-ligands of VEGFR2 namely *lamp3* and *nrp1*, present on the CD8-T_{TEX} surface responsible for triggering this entire phenomenon was evaluated. RT-PCR analysis revealed both of them to be upregulated in T_{TEX}-CSCs. To confirm their possible role, *lamp3* and *nrp1* was silenced via target-specific small-interfering-RNA (siRNA) on T_{TEX} cells. Co-culture was conducted with silenced and non-silenced T_{TEX} with MCF7 cells in presence or absence of VEGFR2i. The silencing lowered CSC frequency, tumorsphere count and redistribution of CXCR4 as well. Cumulatively, these findings validates the involvement of LAMP3/NRP1-VEGFR2 axis in T_{TEX} mediated CSC generation and aggravation.

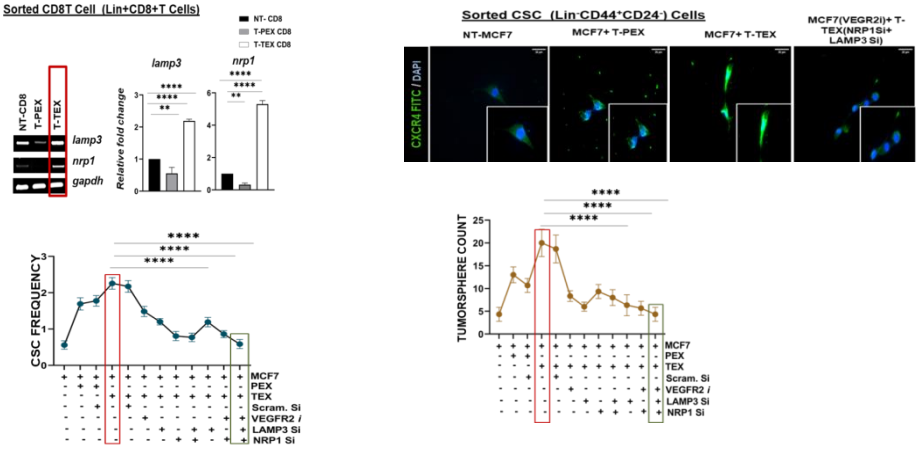

Figure 12: T_{TEX} induced CSC aggression is regulated by LAMP3/NRP1-VEGFR2 axis. A. Studying mRNA expression of VEGFR2-ligands on T-$_{TEX}$ surface via RT PCR. Relative fold changes in gene expression displayed via bar-graphs (mean± SD); one-way ANOVA followed by Tukey's multiple-comparison-test (n=5). B. Representative immunofluorescence micrographs of CXCR4 expression within CSC population in NT-MCF7, MCF7 + T-$_{PEX}$/T-$_{TEX}$ and MCF7 (VEGFR2-neutralized) + T-$_{TEX}$ (*lamp3* and *nrp1*siRNA silenced) group. C. Scatterplot displaying % of $CD44^{+}CD24^{-}$ population after siRNA-silencing of *lamp3* and *nrp1* in T-$_{TEX}$ population followed by co-culture with +/- VEGFR2 neutralized-MCF7. Each dot-plot representing mean± SD of respective cohorts; one-way ANOVA followed by Tukey's multiple-comparison-test (n=3). D. Frequency of tumorsphere formation from CSCs isolated from previous siRNA-treatment-co-culture panel (K). Each dot-plot represents mean± SD of each cohort; one-way ANOVA followed by Tukey's multiple-comparison-test (n=3).*p<0.05, **p < 0.01, ***p < 0.001, ****p < 0.0001, ns: not significant are indicated.

Discussion:

Heterogeneity within dysfunctional exhausted $CD8^+$T cells and their implication in tumor progression is poorly understood. In the present report, we identified two different exhausted $CD8^+$T cell sub-populations within human breast and ovarian tumor tissues, designated as, $Lin^+PD1^+TCF1^+T_{PEX}$ (progenitor-exhausted) and $Lin^+PD1^+TCF1^-T_{TEX}$ (terminally-exhausted) cells. These two sub-sets are phenotypically and functionally distinct, exhibiting differential response to PD1 blockade. Our finding corroborates with the preliminary reports of such subsets on human melanoma patients[21]. However, previous studies were centralized on enhancing the therapeutic candidature of T_{PEX} cells without highlighting T_{TEX} cells and their direct impact within TME. Therefore, in the present study, we wished to analyze these dysfunctional T_{TEX} cells and their ramifications on tumor advancement.

Our study disclosed a strong association between dysfunctional exhausted $CD8^+$TIL population and CSCs in breast and ovarian carcinoma, indicating their possible alliance in tumor promotion. Furthermore, it was uncovered that $CD8^+$T cell exhaustion status, early-state-progenitor-exhaustion or late-state-terminal-exhaustion might be dependent on overall immune infiltration or immune-contexture of TME. Moreover, since patient with cold-tumor shows more tumor-aggressiveness with increased T_{TEX} frequency and CSCs with accentuated stem-cell-transcription factors than inflamed-tumor, it can be postulated that weak tumor infiltration of $CD8^+$T cells and their exhaustion state might dictate the clinical outcome. Association of T_{TEX} and CSCs across human and murine metastatic scenario further solidifies this notion. This also corroborates with previous studies where CSC elevation corresponded to poor prognosis and decreased overall survival[22-23].

When this T_{TEX} and CSC kinship was further investigated *in-vitro*, it was surprisingly found that both the exhausted $CD8^+$T cell subsets actively up-regulated CSC population. However, the degree of CSC-elevation varied very weakly between the T_{PEX} and T_{TEX} influenced cohorts. Furthermore, treatment with PD1-PDL-interaction-inhibitor, T_{PEX} induced CSC generation was prohibited; whereas, T_{TEX} induced CSC up-regulation remained unhinged. This is also reflected in other CSC-attributes like tumorigenic potential and stem-cell-regulatory transcription factors. Thus, from our observation it can be speculated that a patient with non-inflamed tumor stroma, with higher frequency of T_{TEX} may not benefit from anti-PD1 therapy.

Furthermore, to assess T_{TEX}'s precise impact on tumor progression, T_{TEX} influenced CSCs were characterized. Strikingly it was found that T_{TEX} influenced CSCs mostly remain in a hybrid EMT/MET state pertaining both epithelial and mesenchymal features. Previously it has been demonstrated that hybrid-E-M-state confers highest plasticity and stemness of CSCs[24-25]. In line with their report, here, we have also found T_{TEX}~CSCs with higher clonogenicity, exhibiting significantly higher rate of hepatic metastasis in athymic nude mice. Interestingly, T_{PEX}~CSCs with mesenchymal traits demonstrated comparatively lower rate of metastasis. Aside from metastatic potentiality, the EMT-MET state may manifest other CSC characteristics; such as overexpression of *twist* in T_{TEX}-CSCs might play multi-faceted role by maintaining stemness via OCT4, by promoting invasiveness and metastasis through sustained development of invadopodia

and drug resistance via SOX2-ABCG2 axis[26-27]. Downregulation of *vimentin* might provide more nuclear flexibility and migration of amoeboid-T_{TEX}-CSCs through confined environments[28].

This EMT-MET dynamicity is heavily reflected in morphology of T_{TEX}-induced-CSCs; displaying invasive architecture through invadopodia development, nuclear and cytosolic elongation and cofilin over-expression. Previous reports dictate that cancer cells, for their invasion and metastasis, typically use invadopodia to mediate focal degradation of extracellular matrix by MMPs[29]. Remarkably, a positive correlation between increased expression of cofilin with proliferation, invasion, migration and reduced overall survival of patients was reported in various forms of cancer, like NSCLC, breast and prostate cancer has been reported before[30]. Complementing these reports, our matrigel invasion assay and RT-PCR analysis revealed T_{TEX} induced CSCs are indeed highly invasive with MMP7 over-expression. Since these invasive CSCs tend to migrate to secondary sites, chemotaxis associated molecules were canvassed. Our notion was further confirmed by increased expression of CXCR4, indicating a possibility of metastatic spread. Surprisingly CXCR4 was found to be heavily localized in nucleus of T_{TEX} induced CSCs. Similar observation was also reported in metastatic renal and colorectal cancer patients, where high nuclear CXCR4 expression, but not cytoplasmic CXCR4 expression, was correlated with poor prognosis and reduced progression free survival[31-32].

Besides, recent reports in human colorectal cancer have highlighted the importance of immune contexture, lymphatic vessel densities and *in situ* T cell infiltrate or immunoscore in determining distant metastasis via DTCs[33]. Here also we observed similar notion. In cold tumors with elevated T_{TEX}~influenced~CSCs a heavy accumulation of flexible invasive DTCs were noted. These DTCs overly infiltrate tumor-draining lymph node (TDLN) through lymphatic vessels and eventually reach to the distant site and initiate hepatic metastasis.

Moreover, T_{TEX}-influenced CSCs also displayed high MDR phenotype with overexpressing drug efflux pump-regulating genes like *abcc1* and *abcb1*, thus, targeting with conventional chemotherapies becomes much more difficult. Earlier reports also suggested a survival benefit of CSCs with acquisition of MRP1 after chemotherapy in brain tumor patients[34]. Thus our observation further solidifies that CSCs residing stably in an intermediate EMT-MET state and co-expressing both E and M markers, are critical for their rapid poly-functionality along with increased drug resistance, invasiveness and metastatic ability.

Since CSC attributes are primarily orchestrated by transcription factors like OCT4, SOX2, KLF4, NANOG[35] etc., their status was evaluated. Results disclosed the significant upregulation of these molecules in T_{TEX}~CSCs, correlating to our previous findings. T_{TEX}~CSCs were also enriched for *aldh1*, which might also contribute in their invasive morphology[36]. Therefore, cumulatively our study demonstrated an important aspect; that T_{TEX} do not lay silently within TME, rather generates a tumor-promoting, highly invasive, aggressive variant of CSC, which are therapeutically resistant.

Finally, since T_{TEX} cells remain an active perpetrator and are non-responsive to anti-PD1 therapy, determining combating strategies are of urgent need. Given this, we explored the involved signaling networks that might have therapeutic implications. Our results are suggestive that T_{TEX} instigates this aggressive CSC generation via contact dependent receptor-ligand

interaction. They involve unorthodox LAMP3/NRP1-VEGFR2 signaling cascade instead of canonical ligand dependent pathways like Notch, Wnt etc.[37]. Our observation ties along with previous reports of positive association of LAMP3 with invasiveness, resistance to chemo- and radio-therapy and overall poor survival in ovarian carcinoma patients[38]. Moreover, according to recent report in human lung cancer, terminally exhausted $CD8^+$T cell population with higher frequency of NRP1 shows negative regulation of anti-tumor immunity[39]. Silencing of the said axis resulted reduction in CSC frequency, tumor-sphere formation and normalized CXCR4 distribution- from nucleus to cytosol. Thereby our observation provides a directive for therapeutic targeting of T_{TEX} induced tumor promotion.

Additionally it is interesting to note that since NOTCH and WNT are linked in their oscillatory pattern to govern stem cell fate determination, they echo similar expression curves[40]. Previous studies have reported NOTCH inhibition activity resulting in increment in VEGFR2, followed by cellular sprouting which ultimately aid in cellular migration[41-42]. In line with these reports here we also observed, T_{TEX} induced CSCs expressing low NOTCH and WNT, overexpressing VEGFR2 and showcasing cellular sprouting in the form of invadopodia which help in metastasis.

Altogether, this study provides mechanistic insights on how heterogeneous exhausted cell subsets differentially modulate cancer stem cell population to drive tumor aggressiveness. Our findings suggest that ultimate therapeutic benefit of ICI therapy depends both on the frequency and exhausted state of infiltrated $CD8^+$T cells. Vicious T_{TEX} not only escape the scythe of PD1 blockade but also simultaneously promote tumor advancement. Thus, in future, T_{TEX} frequency could be used as a potential biomarker for identifying potential non-responder to anti-PD1 therapy. However, our study implies that in patients with poor immune infiltration, neutralization of LAMP3/NRP1 on T_{TEX} cells holds possibility of therapeutic benefit. Accordingly, LAMP3/NRP1 might serve as potential drug targets; which requires thorough validation from large pool of human cancer samples. Future studies are needed to investigate how T_{TEX} evade PD1 blockade even though they over-express PD1. Possible anti-tumor role of other inhibitory receptors in T_{TEX} could also be ascertained.

References:

1. Batlle E, Clevers H. Nat Med. 2017;23:1124–34.
2. Nassar D, Blanpain C. Annu Rev Pathol Mech Dis. 2016;11:47–76.
3. Chaffer CL, Brueckmann I, Scheel C, Kaestli AJ, et al. Proc Natl Acad Sci. 2011;108:7950–5.
4. Auffinger B, Tobias AL, Han Y, et al. Cell Death Differ. 2014;21:1119–31.
5. Lytle NK, Barber AG, Reya T. Nat Rev Cancer. 2018;18:669–80.
6. Najafi M, Mortezaee K, Majidpoor J. Life Sci. 2019;234:116781.
7. Steinbichler TB, Dudás J, Skvortsov S, et al. Semin Cancer Biol. 2018;53:156–67.
8. Papadaki MA, Stoupis G, Theodoropoulos PA, et al. Mol Cancer Ther. 2019;18:437–47.
9. Markowska A, Sajdak S, Markowska J, Huczyński A. Eur J Med Chem. 2017;142:87–94.
10. Huang H, Wang C, Liu F, et al. Clin Cancer Res. 2018;24:4612–26.
11. Todaro M, D'Asaro M, Caccamo N, Iovino F, Francipane MG, Meraviglia S, et al. J Immunol. 2009;182:7287–96.
12. Wherry EJ, Kurachi M. Nat Rev Immunol. 2015;15:486–99.

13. Hashimoto M, Kamphorst AO, Im SJ, et al. Annu Rev Med. 2018;69:301–18.
14. Darvin P, Toor SM, Sasidharan Nair V, Elkord E. Exp Mol Med. 2018;50:1–11.
15. Siddiqui I, Schaeuble K, Chennupati V, et al. Immunity. 2019;50:195-211.e10.
16. Im SJ, Ha S-J. Immune Netw. 2020;20.
17. Jensen EC. Anat Rec. 2013;296:378–81.
18. Schneider CA, Rasband WS, Eliceiri KW. Nat Methods. 2012;9:671–5.
19. Dasgupta S, Ghosh T, Dhar J, et al. Cell Death Differ. Springer US; 2021;28:3052–76.
20. Hendry S, Salgado R, Gevaert T, et al. Part 1: Assessing the host immune response, TILs in invasi. Adv Anat Pathol. 2017;24:235–51.
21. Miller BC, Sen DR, Al Abosy R, et al. Nat Immunol. 2019;20:326–36.
22. Joseph C, Arshad M, Kurozomi S, et al. Breast Cancer Res Treat. 2019;174:387–99.
23. Connor E V., Saygin C, Braley Cet al. J Ovarian Res. 2019;12:112.
24. Liu S, Cong Y, Wang D, et al. Stem Cell Reports. 2014;2:78–91.
25. Jolly MK, Jia D, Boareto M,et al. Oncotarget. 2015;6:25161–74.
26. Izadpanah MH, Abbaszadegan MR, Fahim Y et al,. Cell Mol Biol Lett. 2017;22:33.
27. Eckert MA, Santiago-Medina M, Lwin TM et al,. J Cell Sci. 2017;130(12):2036-2048
28. Lavenus SB, Tudor SM, Ullo MF, et al,. J Biol Chem. 2020;295:6700–9.
29. Kumar S, Das A, Barai A, Sen S. Biophys J. 2018;114:650–62.
30. Chang C, Chang S, Leu J, et al. Oncol Rep. 2019; 42(2):805-816.
31. Maimaiti Y, Tan J, Liu Z, et al. Oncol Lett. 2017;14:2288–94.
32. Wang S-C, Lin J-K, Wang H-S, et al,. Int J Colorectal Dis. 2010;25:1185–91.
33. Bindea G, Mlecnik B, Galon J. Oncoimmunology. 2021;10:1–3.
34. Jin F, Zhao L, Guo Y-J, et al. Brain Res. 2010;1336:103–11.
35. Yang L, Shi P, Zhao G, et al. Signal Transduct Target Ther. 2020;5:8.
36. Yang L, Ren Y, Yu X, et al. Mod Pathol. 2014;27:775–83.
37. Fendler A, Bauer D, Busch J, et al. Nat Commun. 2020;11:929.
38. Wang D, Cao X, Zhang Y, et al. Tumor Biol. 2017;39:101042831769501.
39. Liu C, Somasundaram A, Manne S, et al. Nat Immunol. 2020;21:1010–21.
40. Sonnen KF, Lauschke VM, Uraji J, et al. Cell. 2018;172:1079-1090.e12.
41. Bentley K, Franco CA, Philippides A, et al. Nat Cell Biol. 2014;16:309–21.
42. Meisel CT, Porcheri C, Mitsiadis TA. Cells. 2020;9:1879.

13. Hashimoto M, Kamphorst AO, Im SJ, et al. Annu Rev Med. 2018;69:301–18.
14. Darvin P, Toor SM, Sasidharan Nair V, Elkord E. Exp Mol Med. 2018;50:1–11.
15. Siddiqui I, Schaeuble K, Chennupati V, et al. Immunity. 2019;50:195-211.e10.
16. Im SJ, Ha S-J. Immune Netw. 2020;20.
17. Jensen EC. Anat Rec. 2013;296:378–81.
18. Schneider CA, Rasband WS, Eliceiri KW. Nat Methods. 2012;9:671–5.
19. Dasgupta S, Ghosh T, Dhar J, et al. Cell Death Differ. Springer US; 2021;28:3052–76.
20. Hendry S, Salgado R, Gevaert T, et al. Part 1: Assessing the host immune response, TILs in invasi. Adv Anat Pathol. 2017;24:235–51.
21. Miller BC, Sen DR, Al Abosy R, et al. Nat Immunol. 2019;20:326–36.
22. Joseph C, Arshad M, Kurozomi S, et al. Breast Cancer Res Treat. 2019;174:387–99.
23. Connor E V., Saygin C, Braley Cet al. J Ovarian Res. 2019;12:112.
24. Liu S, Cong Y, Wang D, et al. Stem Cell Reports. 2014;2:78–91.
25. Jolly MK, Jia D, Boareto M,et al. Oncotarget. 2015;6:25161–74.
26. Izadpanah MH, Abbaszadegan MR, Fahim Y et al,. Cell Mol Biol Lett. 2017;22:33.
27. Eckert MA, Santiago-Medina M, Lwin TM et al,. J Cell Sci. 2017;130(12):2036-2048
28. Lavenus SB, Tudor SM, Ullo MF, et al,. J Biol Chem. 2020;295:6700–9.
29. Kumar S, Das A, Barai A, Sen S. Biophys J. 2018;114:650–62.
30. Chang C, Chang S, Leu J, et al. Oncol Rep. 2019; 42(2):805-816.
31. Maimaiti Y, Tan J, Liu Z, et al. Oncol Lett. 2017;14:2288–94.
32. Wang S-C, Lin J-K, Wang H-S, et al,. Int J Colorectal Dis. 2010;25:1185–91.
33. Bindea G, Mlecnik B, Galon J. Oncoimmunology. 2021;10:1–3.
34. Jin F, Zhao L, Guo Y-J, et al. Brain Res. 2010;1336:103–11.
35. Yang L, Shi P, Zhao G, et al. Signal Transduct Target Ther. 2020;5:8.
36. Yang L, Ren Y, Yu X, et al. Mod Pathol. 2014;27:775–83.
37. Fendler A, Bauer D, Busch J, et al. Nat Commun. 2020;11:929.
38. Wang D, Cao X, Zhang Y, et al. Tumor Biol. 2017;39:101042831769501.
39. Liu C, Somasundaram A, Manne S, et al. Nat Immunol. 2020;21:1010–21.
40. Sonnen KF, Lauschke VM, Uraji J, et al. Cell. 2018;172:1079-1090.e12.
41. Bentley K, Franco CA, Philippides A, et al. Nat Cell Biol. 2014;16:309–21.
42. Meisel CT, Porcheri C, Mitsiadis TA. Cells. 2020;9:1879.

Anamika Bar.
30/8/2023